High-Strength Alloyed Steel: Modelling Dynamic and Multiaxial Loading Conditions

Antonina Trippel[1], Wilfried Harwick[2]

[1]Institut für nachhaltige technische Systeme - INATECH
[2]Fraunhofer Ernst-Mach-Institut (EMI)

1 Abstract

This work reports on the modelling of failure behaviour in case of a high strength alloyed steel, experimentally subjected to a range of strain rates and states of stress triaxiality. This material combines high strength with exceptionally high ductility, which makes it difficult to describe material behaviour based on well-known constitutive models such as Johnson-Cook [1] [2].
To solve this challenge, extensive experimental investigations were performed to record stress-strain relations and, in particular, failure behaviour. Different states of triaxiality were attained based on the specimen geometry. Experiments with flat, unnotched and notched specimens yielded triaxial stress-states under uniaxial loading conditions. Stress-states due to shear stress and combinations of shear and tensile stresses were studied with biaxial tensile specimens.
The triaxiality of the uniaxial tensile specimens was calculated based on the approximation suggested by Bridgman [3]. Based on the detected data, the material models suggested by Johnson-Cook [1] [2] was parameterized. Parameterization was carried out with the software LS-OPT [5]. The parameters of the constitutive models were found in an optimization procedure which minimized the difference between simulation prediction and experimental results.
The discretization and element size was varied in order to study discretization effects. Smaller element sizes enabled a more constant triaxiality over the duration of the simulation.
The parameter space of the Johnson-Cook model allowed for a satisfactory agreement in case of uniaxial experiments with a value of the stress triaxiality ≥ 1/3. However, the more complex problem of accurately modelling failure at other values of stress triaxiality between 0 (pure shear) and 1/3 (uniaxial tension) could not be solved. We discuss possible reasons for the apparent inability of the Johnson-Cook failure model to describe the effects induced by triaxiality at large failure strains and under shear stresses.

2 Introduction

Structural optimization towards lower weight and higher load capabilities is a key issue in the process of energy and resources. Inherent to this process is an increased complexity of the involved materials, structures and loading conditions. Load applications become more complex and require more intricate models to describe the full spectrum of material behavior. Elastic, plastic, damage and failure states of the material have to be taken into consideration.
Over the years, an array of numerical material models has been established in order to simulate a variety of systems. A model is a simplified depiction of the reality. Numerical models predict material behavior in a large number of situations based on the insights obtained prior by experiments. Especially the accurate depiction of damage and failure requires sophisticated models, which include an array of influences such as strain rate and temperature. Multiaxiality of the stress state is a key factor relevant for damage initiation and the resulting failure of a system. The stress state describes the load on a point of any given material. The description, quantification and implementation of stress triaxiality into a material model provide a more reliable description of the material behavior. Choosing the right material model for a certain situation is fundamental for the right prediction of system's behavior.
Depending on the application, simulation errors can be fatal. Therefore, the numerical model not only has to depict all influences the material is affected by, but also calculate and assess the corresponding weighting of those influences.
This paper's main objective is to provide an overview of the characterization and modeling process of a given material. The overview showcases the current state of the material characterization and modeling.

3 Multiaxial Stress State

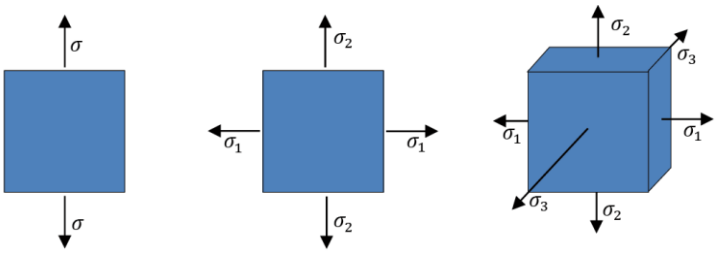

Fig.1: Abstract representation of different stress states in dependency on the load σ or the principal stresses σ_1-σ_2-σ_3. On the right is an exemplary representation of a uniaxial stress state in a two-dimensional case. In the middle is a biaxial stress state in a two-dimensional case. On the left is a triaxial stress state in a three-dimensional case.

The load on a point in any given material is described by a state of stress. The state of stress can be uniaxial or multiaxial. In a two-dimensional case, the multiaxial state of stress is called biaxial, in a three-dimensional case it is defined as triaxial (Fig.1).
The state of stress is dependent on the material properties and its internal structure. Additionally, the geometry and the point of attack of the force are to be considered.
Stress triaxiality is relevant for failure initiation. The analysis of specimens particularly designed to invoke a single type of stress state – so it can be looked at in isolation – allows to understand possible failure mechanisms and to design resilient constructions.
In order to compare different states of stress, stress triaxiality has to be described qualitatively and quantitatively. The triaxiality factor is often used as a parameter in failure models in order to describe the connection between failure and stress state. [6]

3.1 Triaxiality Factor

The triaxiality factor η is a scalar parameter, which represents the amount of multi-axiality of a stress state. It describes the hydrostatic part of the Cauchy stress tensor and characterizes the void growth in a material. The factor is the ratio of the hydrostatic stress p or mean stress σ_m and the von Mises equivalent stress σ_{vM}. [7] [8]

$$\eta = \frac{\sigma_m}{\sigma_{vM}} = \frac{-p}{\sigma_{vM}} = \frac{\frac{1}{3}(\sigma_1+\sigma_2+\sigma_3)}{\sqrt{\frac{1}{2}[(\sigma_1-\sigma_2)^2-(\sigma_2-\sigma_3)^2-(\sigma_3-\sigma_1)^2]}} \tag{1}$$

3.2 Approximation of the Triaxiality Factor

Although triaxiality can be calculated using principal stresses, this method is mostly not applicable for experimental results due to the lack of information. Bridgman et al. [3] suggested an approximate solution for a necked plane strain specimen:

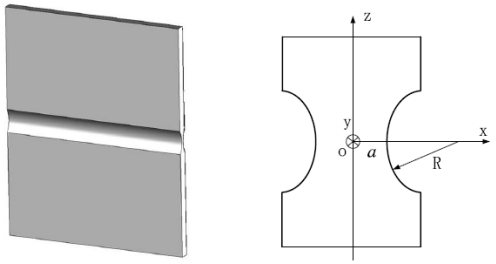

Fig.2: Sketch of a flat-grooved plane strain specimen (l.) and its cross section (r.), with t = 2a as the ligament thickness and R as the radius at the notch root. [9]

$$\eta = \frac{\sqrt{3}}{3}\left[1+2\ln\left(1+\frac{a}{2R}\right)\right] = \frac{\sqrt{3}}{3}\left[1+2\ln\left(1+\frac{t}{4R}\right)\right] \tag{2}$$

The factor $t = 2a$ is the ligament thickness of the flat specimen. The equation is based on the presupposition that the stress triaxiality at the center of a specimen is $\eta \geq 1/\sqrt{3}$ and a rigid-perfect plastic condition is present. Furthermore, the Lode angle parameter $\bar{\theta}$ is proven to remain zero. [9]

4 Material Model: Johnson-Cook

The Johnson-Cook Model [10] is a typically used phenomenological model due to its implemented strain rate and temperature dependency. Additionally, the fracture model [11] combines different loading cases and combinations through utilizing the triaxiality factor η. This makes the model versatile and applicable to different loading scenarios. The model is divided in the yield and the fracture model.
The yield model describes the yield stress in dependency of the equivalent plastic strain $\bar{\varepsilon}_p^n$, plastic strain rate $\dot{\bar{\varepsilon}}_p^*$ and temperature T. The strain hardening, strain rate and temperature dependency are described by the parameters σ_0 (alternatively A), B, n, C, m:

$$\sigma_Y=(\sigma_0+B\bar{\varepsilon}_p^n)(1+C\ln\dot{\bar{\varepsilon}}_p^*)(1-T^{*m}) \quad (4)$$

The fracture model presupposes that the critical equivalent plastic strain $\bar{\varepsilon}^f$ is a monotonously decreasing function of the stress triaxiality η (Fig.3). The postulated criterion for failure is described by five material constants D_1-D_5:

$$\bar{\varepsilon}^f=(D_1+D_2\exp(D_3\eta))(1+D_4\ln\dot{\varepsilon}_{pl}^*)(1+D_5T^*) \quad (5)$$

The first three parameters of each model can be derived from quasi-static tension tests with a constant strain rate. The strain rate parameter requires dynamic tensile tests with varying strain rates. The third term is often omitted.

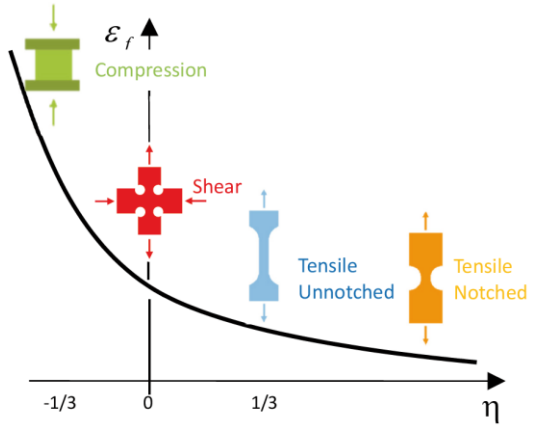

Fig.3: Failure strain over triaxiality factor according to Johnson-Cook. The main loading conditions are marked with its corresponding specimen geometries. [12]

5 Methodology of Material Characterization

The material chosen for characterization is a steel type 30NiCrMoNb5 for civil applications. It is a high strength alloyed steel used for protective purposes. The material combines ductile behavior with a comparatively high ultimate tensile strength. The analysis of the multiaxial stress state and the strain rate influence yields a base to describe and simulate materials with a similar composition and similar characteristics. This aids the prediction of the material's response in case of high loads.

5.1 Testing Plan

In order to characterize the material and gain basic material data like Young's modulus, yield stress, fracture stress and fracture strain, flat tensile specimens are used. The tensile specimens are divided into unnotched and notched specimens. The unnotched specimens are used to define the basic mechanical parameters of the material. The notched specimens induce a multiaxial stress state and show the dependency of the material on the stress triaxiality. Varying strain rates provide information about the strain rate dependency with regard to the aforementioned basic material data. Since the base material was available in sheets only, flat tensile specimens are used (Fig.4).
The notched specimens have radii of 2 mm, 5 mm and 10 mm. The test runs are subjected to be performed at strain rates of 0.01 1/s (quasi-static), 1.0 1/s and 100 1/s. For every strain rate and type of specimen, 5 specimens are tested. This yields 60 test runs in total. For every test scenario, at least 3 valid tests are needed.
The geometry of the tensile specimens is based on DIN 50125 Form E. The clamp areas were adjusted to the specifications of the mounting devices of the tensile test setup. In order to reduce the force needed for failure and possible oscillations, the cross-sectional area was reduced to a maximum

of 8 mm². This ensures the failure of the specimen and counteracts oscillations by reducing the shock drop of the force at failure.
Additionally, tests with an infrared camera are performed in order to depict the degree of temperature dependency. Due to time limitations, a full array of temperature dependency tests could not be performed.

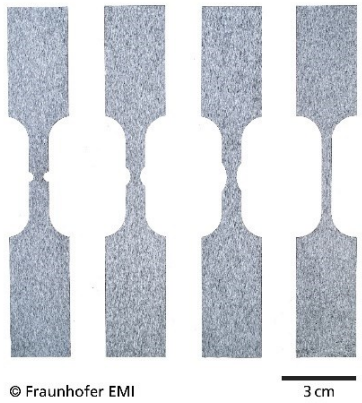

Fig.4: Overview over the flat tensile specimens with radii of 2 mm, 5 mm, 10 mm and unnotched (l.t.r.)

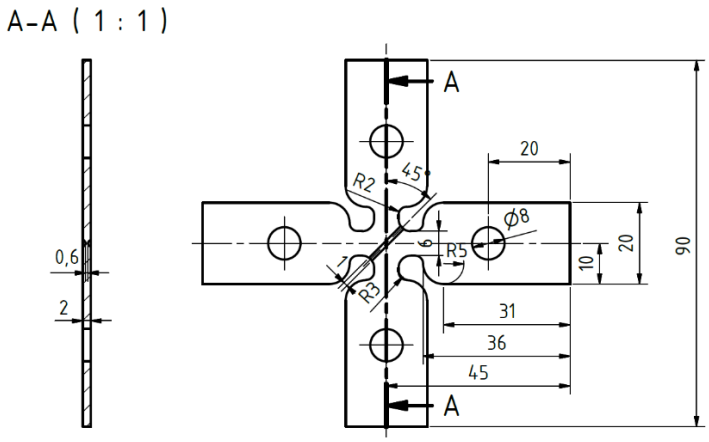

Fig.5: Geometry of a biaxial tensile specimen with a 45° notch.

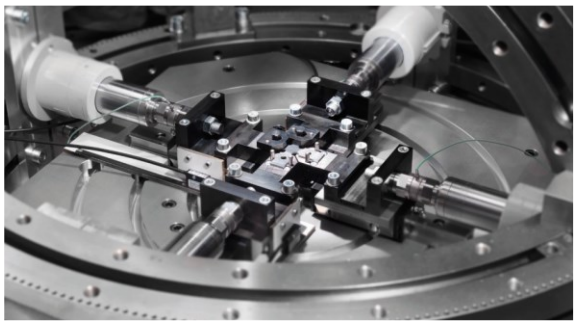

Fig.6: Biaxial tensile testing setup.

To investigate the material behavior under shear stresses, cross-shaped biaxial specimens are used. This specimen geometry has been chosen for two reasons: Alternatives such as the Arcan-specimen developed by Arcan et al. [13], which are influenced by simple shear, often fail not due to the shear stress, but rather due to tensile stress on the fringes of the measurement section. Additionally, notching the specimens opens the possibility to influence the stress-state and to investigate pure shear, shear-tensile and shear-compressive stresses.
The geometry (Fig. 5) is based on the specification of the used biaxial setup (Fig. 6). The cross-section at the notch is selected with the tensile strength of the material and the machines maximum forces taken into consideration. The size of the notch results in a predicted fracture surface of less than 8 mm². This ensures the failure of the specimen within the machine limitations as well. Placing

the notch in a 45°- angle results in pure shear stresses. Additionally, specimens with a 60°-angle are manufactured in order to describe the material behavior for a combination of shear and tensile stresses.

5.2 Test Analysis

In order to analyze and compare the results, force over time and displacement over time are synchronized utilizing the time data. From force and displacement data, the stress-strain curve is derived. The force signal is obtained from a strain gauge based load cell or piezoelectric sensors. The displacement and therefore the strain are measured via DIC (Fig.7, l.).

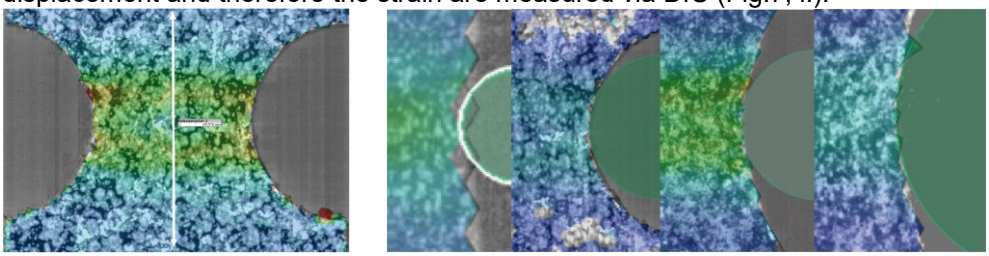

Fig.7: Optical extensometer on a notches specimen with an initial radius of 2 mm as utilized in GOM Correlate (l.). The extensometer yields the displacement and the strain. On the right, radii shortly before failure of unnotched and notched specimens with 2 mm, 5 mm and 10 mm initial radius (l. t. r.) as tracked in GOM Correlate

The change of the radius of the notch over the course of a test up to the point of failure is analyzed on the surface of the flat specimens. Three points on the edge of the specimen are selected. Those points approximate the inner radius around the point of failure (Fig.7, r.). This allows for the monitoring of the deformation of the notch and the change of the radius up to the point of failure.

6 Experimental Results

At strain rate of 0.01 1/s (Fig.8) the material yields at 1300 MPa, as predicted by the data sheet. The ultimate tensile strength reaches a value of around 1824 MPa followed by a decline until the specimen fails. The measured tensile strength is higher than the value given in the data sheet of the material. The curves of different specimens show a similar path up until the point of ultimate tensile strength. This indicates a high level of reproducibility. The failure strains deviate within a strain interval from 0.082 to 0.087. The failure strain is similar to the failure strain given by the data sheet. The local stresses reach higher values of over 2000 MPa in comparison to its global counterpart. Additionally, the local strains get as high as 0.48 in comparison to the global strains, which reach only a value of about 0.09. The curves gained in a series of tests at a strain rate of 1.0 1/s show a similar development (Fig.9).

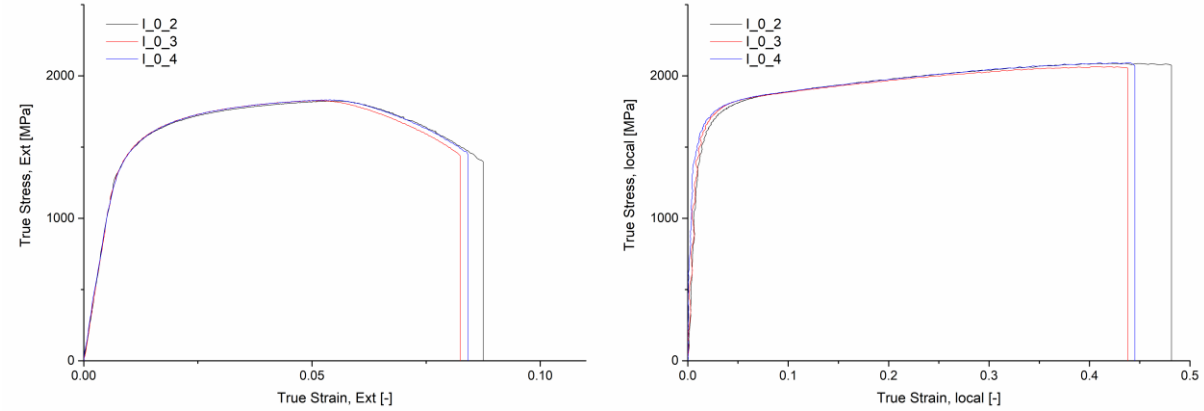

Fig.8: Global (l.) and local (r.) true stress over true strain of an unnotched specimen at 0.01 1/s.

Overlaid plots of different strain rates yield that the material experiences lower fracture strains and stresses at the higher of the two strain rates (Fig.10). This might be the result of softening due to the strain rate, temperature, or a combination of both.
The force signals obtained at a strain rate of 100 1/s were highly prone to oscillation. Due to this high oscillation, no accurate results could be obtained. In order to counteract the oscillation, the test setup has to be highly modified.

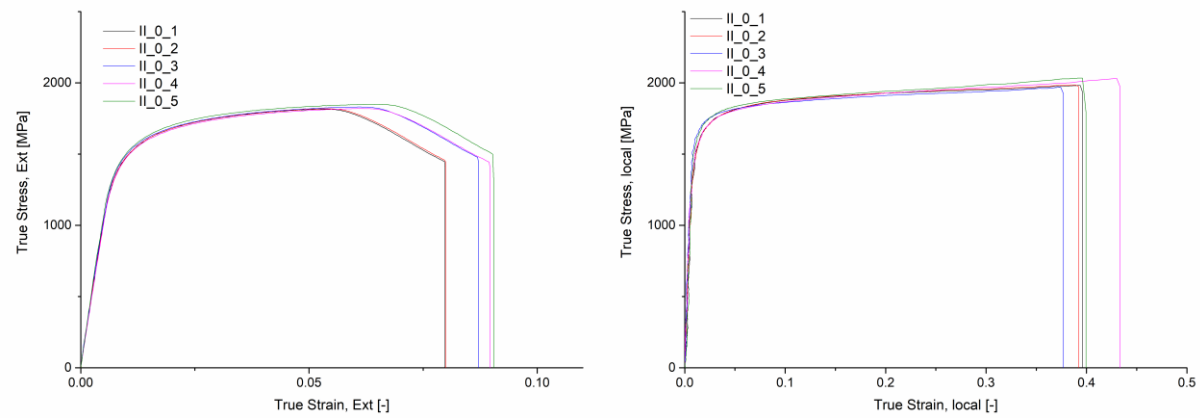

Fig.9: Global (l.) and local (r.) true stress over true strain of an unnotched specimen at 1.0 1/s.

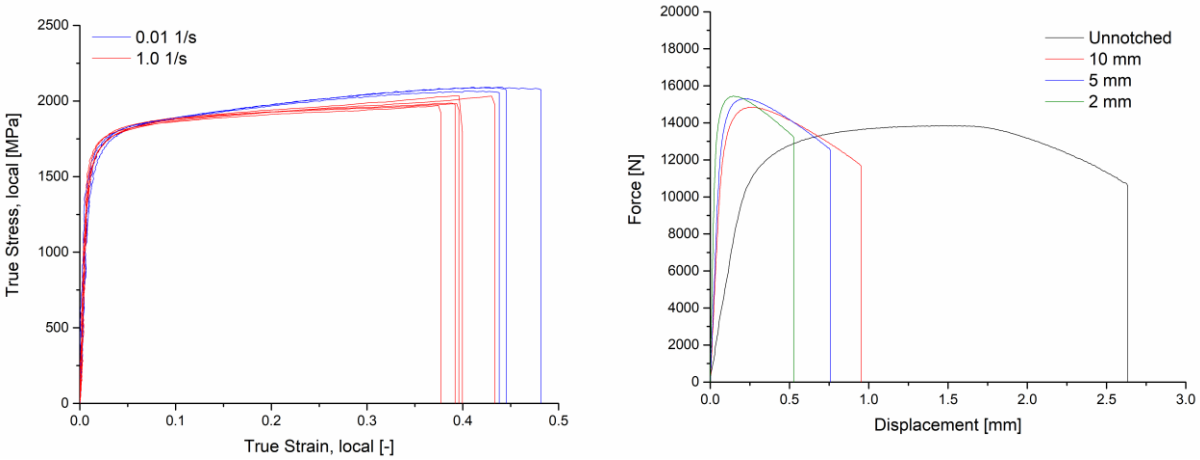

Fig.10: On the left, softening of the material at growing strain rates. On the right, comparison of forces over displacement of unnotched and notched specimens at 0.01 1/s.

The force over the displacement provides an overview of the measured results of all uniaxial geometries (Fig.10). The difference in slope in the elastic section is due to the difference in radii, since the initial cross-sectional area is identical for all types of tensile specimens. The lower the radius, the less deformation the specimen of the tested material can experience until failure occurs. The lower the notch radii, the higher is the ultimate force and the lower is the failure strain.

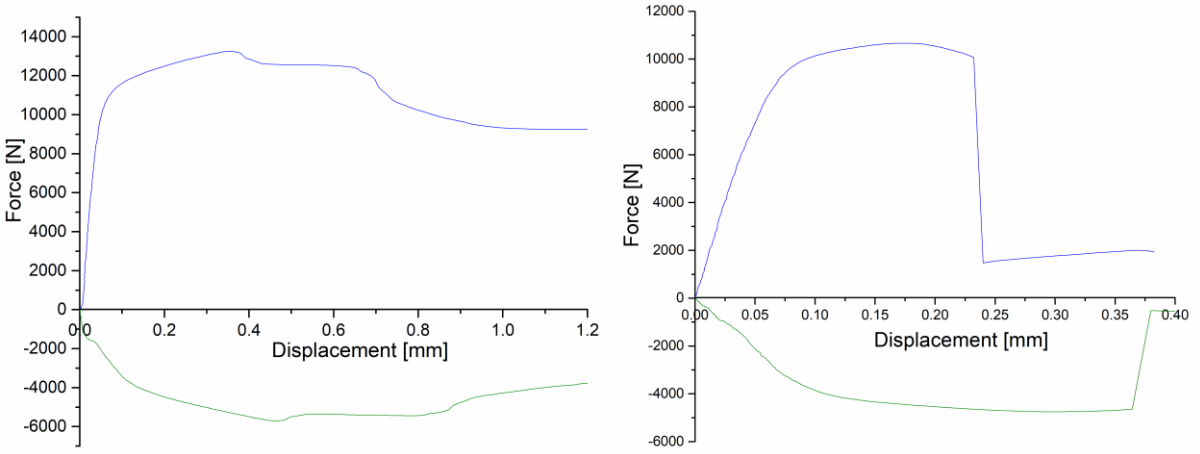

Fig.11: Average tensile (blue) and compressive (green) force over absolute displacement in case of a biaxial specimen with a 45°-notch (l.) and a 60°-notch (r.). On the left, the indicator for failure is the first dip in force.

In case of the biaxial tensile specimens (Fig.11), the force in compressive and tensile direction is the average force signal of both actuators in lateral or longitudinal direction. The difference in

displacement between the longitudinal and the transversal direction is a result of a deviation in velocity. The deviation is a result of bending in the actuators due to the reciprocal transverse forces.

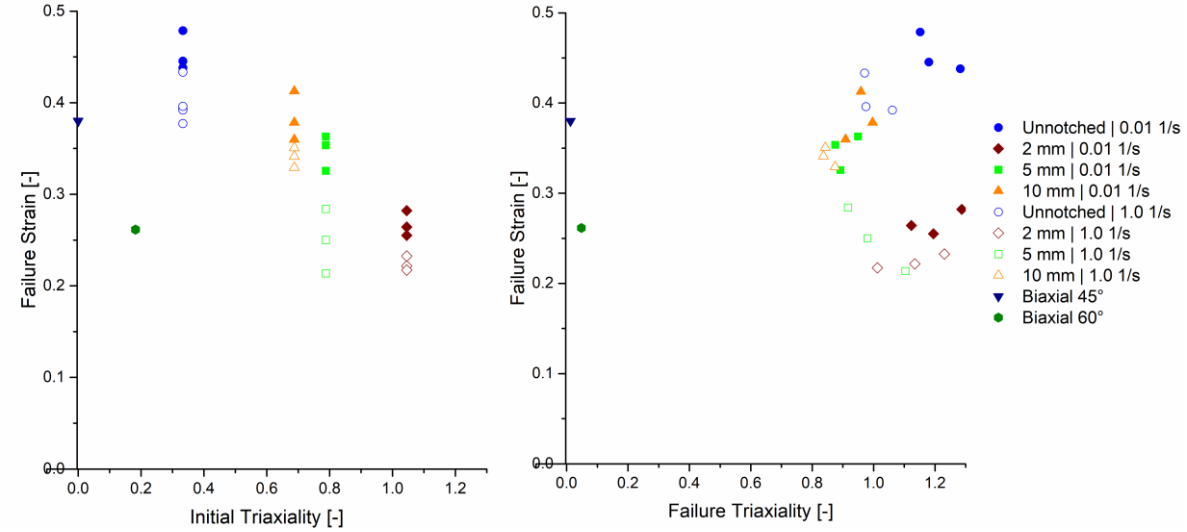

Fig.12: Failure strain over initial triaxiality (l.) and over failure triaxiality (r.) of the tested specimen geometries at two different strain rates. The uniaxial specimens follow the path predicted by Johnson-Cook, while the biaxial specimens do not follow this rule. At the point of failure the triaxialities tend to overlap due to the high ductility of the material, which results in a cluster.

The triaxialities of the tensile tests were calculated using the approximation suggested by Bridgman [9]. The biaxial triaxialities were approximated presupposing the stresses in tensile and compressive direction as the first two principal stresses neglecting the third. The data of this material yields triaxialities higher than expected for the unnotched specimens, which overlap with the results of the lowest radii of 2 mm (Fig.12). This results in a cluster. This does not allow to assess a correlation. The results of the biaxial tests indicate that the material does not follow the path established by Johnson-Cook.

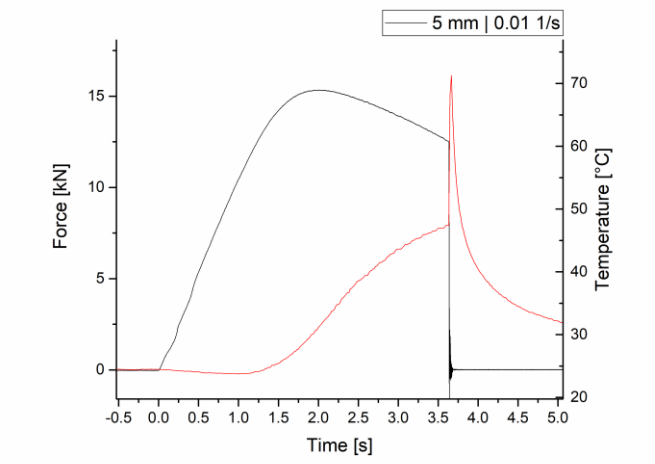

Fig.13: Force (grey) and temperature (red) over time of a notched specimen with an initial radius of 5 mm at 0.01 1/s. The temperature experiences an increase around the point of failure.

The temperature plot (Fig.13) is influenced by a time delay due to the heat transfer. The notched specimen experiences a cooling effects due to thermoelastic effects in the range of elastic deformation. After the yield point, the temperature rises with increasing plastic deformation. The temperature reaches up to about 45 °C. The specimen experiences high plastic deformation prior to its failure, which results in an instantaneous rise in temperature to over 70 °C. The results support the theory of material softening due to the influence of temperature. Due to time limitation, this influence cannot be depicted adequately. Therefore, temperature influence is neglected in the course of this work.

7 Numerical Simulation

The parameters were obtained via data fitting and LS-OPT and later compared.
In case of data fitting a hardening curve was defined. The parameters were determined using the method of least squares (Fig.14). The parameters of the fracture model were obtained by using the triaxiality results (Fig.15). The results of the biaxial tests were neglected due to non-conformity with the Johnson-Cook model. The calculation based on the failure triaxialities was not possible due to the cluster formed by overlapping data. The curves align with the results for the initial triaxialities, but do not represent the necking of the specimens at the point of failure.
Alternatively, the model was fitted to the force over strain curves via LS-OPT. The calculation implemented the results of all uniaxial geometries and strain rates.

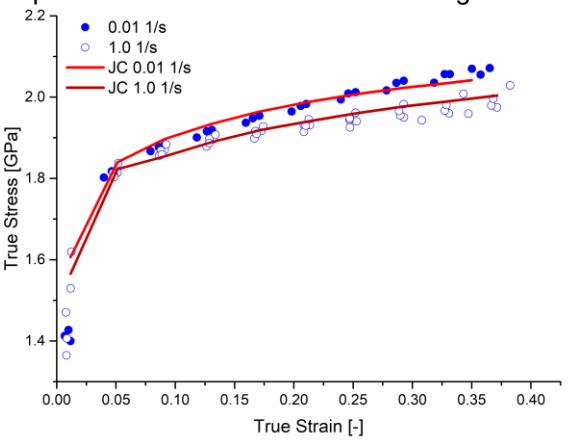

Fig.14: Experimental true stresses over true strains and calculated Johnson-Cook yield functions at 0.01 1/s and 1.0 1/s, respectively. The fitting of the yield function was achieved using the method of least squares.

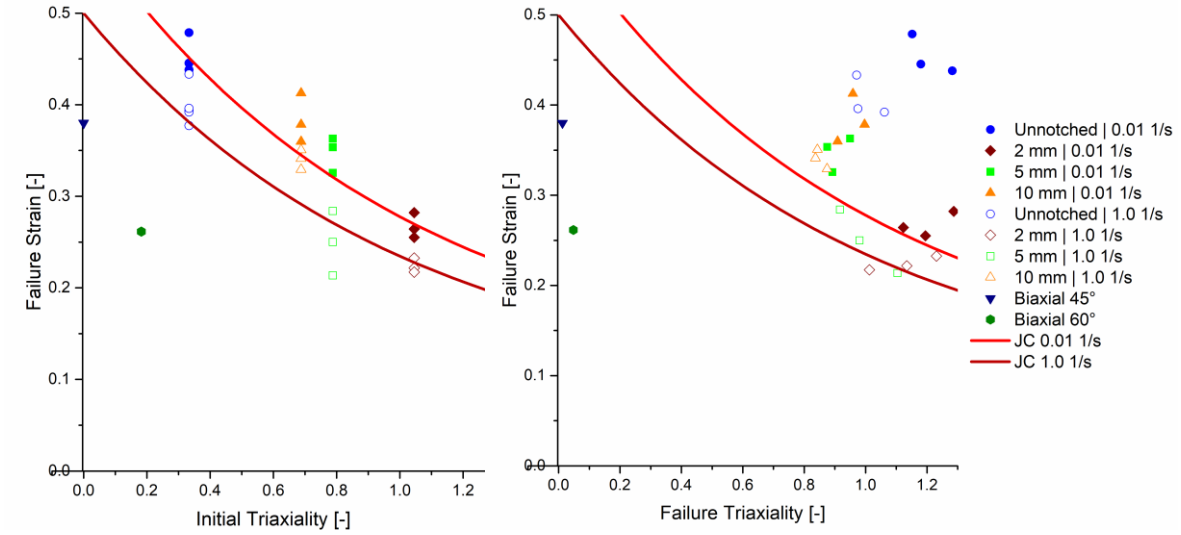

Fig.15: Experimental failure strains over initial triaxialities (l.) and failure triaxialities (r.) and calculated Johnson-Cook curves at 0.01 1/s and 1.0 1/s, respectively. The result does match the initial triaxialities, but not the failure triaxilities.

The results of the simulation with parameters calculated via data fitting (Fig.16, l.) do not align with the results obtained by the tests. The failure resembles brittle failure. Manual optimization of the simulation is inefficient, inaccurate and yield satisfactory results. Therefore, in this particular case, data fitting based on the test results obtained prior does not yield a simulation which represents the material behavior of the material tested.
On the other hand, the simulation with parameters calculated via LS-OPT (Fig.16, r.) manages to depict the material behaviour. The simulation predicts material failure at higher failure forces and failure strains in case of the unnotched specimens and at higher failure strains for the notched specimens. This deviation might be a result of the missing temperature dependency in the model. The

deviation decreases with increasing specimen radii. The calculated parameters resemble the values expected.

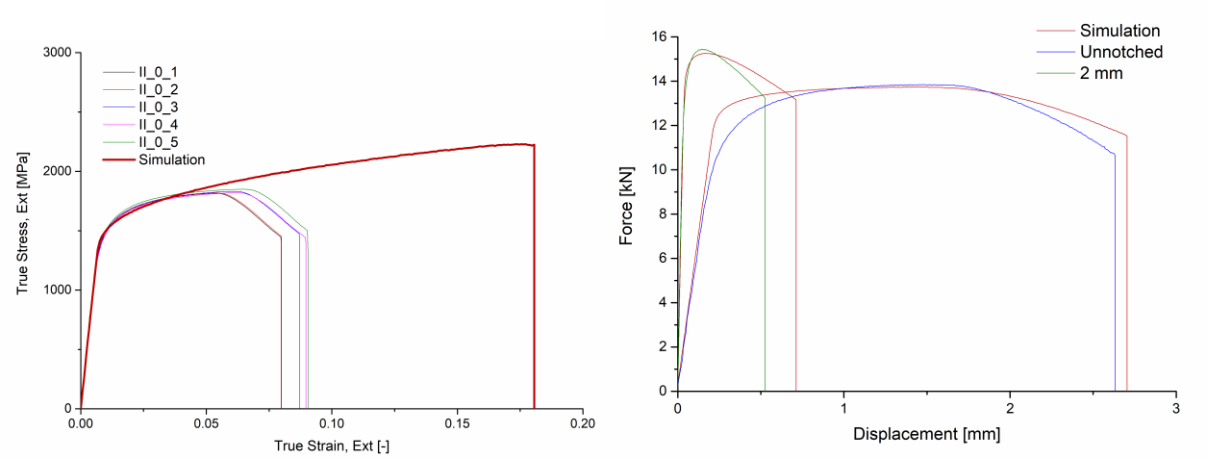

Fig.16: On the left, global true stress over true strain of the simulation with parameters calculated via data fitting and the test results of unnotched specimens. The results of the simulation do not align with the results obtained by the tests. In comparison, on the right results LS-OPT Johnson-Cook with 1.0 1/s strain rate. The curves show the results of the unnotched specimens and notched specimens with a radius of 2 mm in order to provide an overview.

The simulation results of LS-OPT were used to depict the steadiness of the triaxiality over the duration of the simulation (Fig.17). The first element to fail in the section of the notch was analyzed. The tensile and shear stresses were used to calculate the three principal stresses and to calculate the triaxiality of the element at the point of failure precisely. This simulation yields a more constant triaxiality over the duration of the simulation with decreasing element size. Additionally, the triaxiality of the unnotched specimen stays constant but increases significantly shortly before the point of failure. This aligns with the material behavior observed in the experimental results. The simulation yields an overlap of the failure triaxialities and results in a cluster as well. This means that even though the parameters were not directly based on phenomena observed prior and were derived mathematically via LS-OPT, the simulation still resembles the behavior described by the tests closely.

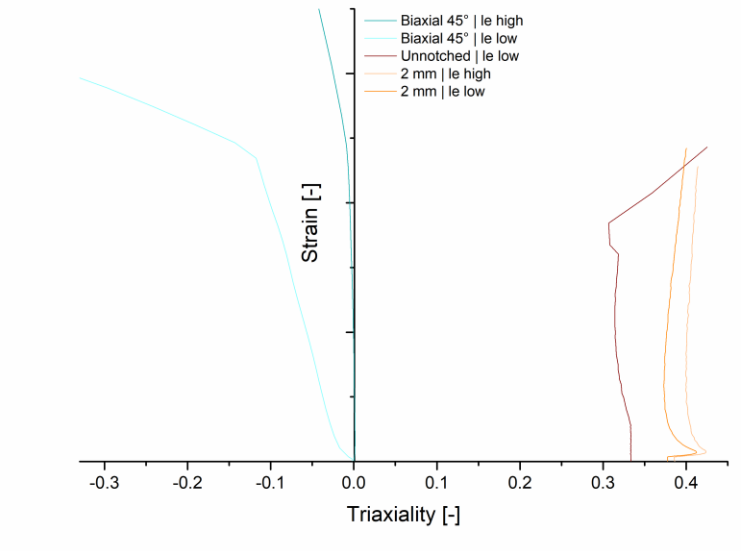

Fig.17: Steadiness of the triaxiality factor. Lower element sizes result in a more steady triaxiality over the duration of the simulation. The failure triaxialities tend to overlap and yield results that closely resemble the overlap of the test results.

Simulations with the calculated parameters of the models of the biaxial specimens do not represent the material behavior depicted by the test results (Fig.18). The simulation fails at higher strains and lower stresses compared to the results of the material tests. This issue was expected based on the nonconformity of the test results with the Johnson-Cook model. Therefore other models have to be implemented, such as Bao-Wierzbicki [14] and Xue-Wierzbicki [15].

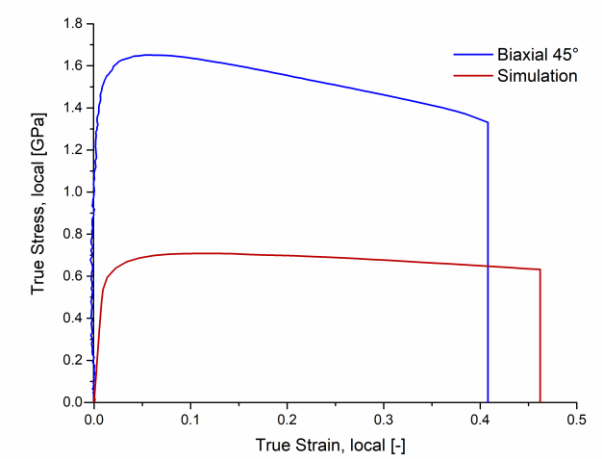

Fig.18: Comparison result of biaxial tensile test with a 45°-notched specimen and the simulation in tensile direction. The simulation predicts lower stresses and fails at higher strains.

8 Summary and Conclusion

In order to provide material parameters and to investigate the influences of stress triaxiality and strain rate, an array of material tests was performed. The material characterized was a high strength steel. The specimens used were unnotched and notched flat tensile and biaxial specimens. The results yielded material behavior under pure shear, shear-tensile and tensile stresses with different multiaxial stress-states. The displacement and the corresponding strain were obtained via DIC and synchronized with the force signal. Triaxiality was estimated using an approximation formula by Bridgman [3]. The material yields increasing tensile strength and decreasing failure strain with decreasing notch radii. An influence of strain rate could be established up to a strain rate of 1.0 1/s. Higher strain rates yielded non-analyzable results due to high oscillations. The strain rate analysis yielded an increasing softening of the material with increasing strain rates. However, potential temperature dependency was established and might be the cause for the softening of the material. The initial triaxiality of the material yielded the results expected. The failure triaxialities of the specimens overlapped due to necking and did not allow to assess a correlation. Additionally, the results of the biaxial specimens did not follow the same dependency of triaxiality as the flat tensile specimens.
Based on the results obtained, a numerical simulation was performed. The parameters for the Johnson-Cook model were first calculated via data fitting. The results were inaccurate and the parameters could not depict the damage and failure behavior experienced during the tests. An optimization with LS-OPT yielded more accurate results. One parameter set was able to detect the behavior of all flat tensile specimens with an acceptable deviation. An analysis of the parameters and the steadiness of the triaxiality showed a similar material behavior to the one already seen in the results of the material characterization. As predicted, the model was not able to depict the behavior under shear and shear-tensile stresses and needs to be extended or replaced by a model which describes this range of triaxiality accurately, such as Bao-Wierzbicki [14] and Xue-Wierzbicki [15].

9 Literature

[1] Johnson, G. R., Cook, W. H.: "A Constitutive Model and Data for Metals Subjected to Large Strains, High Strain Rates and High Temperatures", Proceedings to the Seventh International Symposium on Ballistics, Den Haag, 1983
[2] Johnson, G. R., Cook, W. H.: "Fracture Characteristics of Three Metals Subjected to Various Strains, Strain Rates, Temperatures and Pressures", Engineering Fracture Mechanics 21, pp. 31-48, 1985
[3] Bridgman, P.: “Studies in large Plastic Flow and Fracture”, New York: McGraw Hill, 1952
[4] Jiang, W., Li, Y., Shu, Y., Fan, Z.: "Analysis of Metallic Ductile Fracture by extended Gurson models", 13th International Conference on Fracture, June 2013
[5] LSTC: "LS-OPT", [Online]. Available: http://www.lstc.com/products/ls-opt. [Accessed 19 September 2018]
[6] Marcadet, S.J., Roth, C.C., Erice, B., Mohr, D.: “"A rate-dependent Hosford-Coulomb model for predicting ductile fracture at high strain rates", EDP Sciences, 2015
[7] Mohr, D.: "Dynamic behaviour of materials and structures. Lecture #7", ETH Zürich, Fall 2015

[8] Hiermaier, S.: "Physics of Failure - Lecture #11", Sustainable Systems Engineering – INATECH, Freiburg im Breisgau, 2017
[9] Bai, Y., Teng, X., Wierzbicki, T.: "On the Application of Stress Triaxiality Formula for Plane Strain Fracture Testing", Journal of Engineering Materials and Technology, April 2009
[10] Johnson, G.R. and Cook, W.H.: "A Constitutive Model and Data for Metals Subjected to Large Strains, High Strain Rates and High Temperatures", in Proceedings to the Seventh International Symposium on Ballistics, Den Haag, 1983
[11] Johnson, G.R. and Cook, W.H.: "Fracture Characteristics of Three Metals Subjected to Various Strains, Strain Rates, Temperatures and Pressures", Engineering Fracture Mechanics 21, pp. 31-48, 1985
[12] Jansen,J.: "Ein Werkstoffmodel für eine Aluminium-Druckgusslegierung unter statischen und dynamischen Beanspruchungen - Ph.D.", 2007
[13] Arcan, M., Hashin, Z., Voloshin, A.: "A Method to Produce Uniform Plane-Stress States With Application to Fiber-Reinforced Materials" in Experimental Mechanics 18, pp. 161- 178
[14] Bao, Y., Wierzbicki, T.: “On Fracture Locus in the Equivalent Strain and Stress Triaxiality Space", International Journal of Mechanical Science 46, pp. 81-98
[15] Xue, L., Wierzbicki, T.: "Verification of a New Fracture Criterion Using LS-DYNA"